Wide-spread brain activation and reduced CSF flow during avian REM sleep

Gianina Ungurean
Max Planck Institute for Biological Intelligence (in foundation)
Mehdi Behroozi (mehdi.behroozi@ruhr-uni-bochum.de)
Ruhr Universität Bochum https://orcid.org/0000-0001-8373-6168
Leonard Boeger
Max-Planck-Institute for Neurobiology of Behavior https://orcid.org/0000-0002-0964-4991
Xavier Helluy
Ruhr-University Bochum
Paul-Antoine Libourel
Université Claude Bernard Lyon 1 https://orcid.org/0000-0001-6726-5829
Onur Gunturkun
Ruhr-Universität Bochum https://orcid.org/0000-0003-4173-5233
Niels Rattenborg
Max Planck Institute for Biological Intelligence (in foundation)

Article

Keywords:

Posted Date: November 23rd, 2022

DOI: https://doi.org/10.21203/rs.3.rs-2170252/v1

Abstract

Mammalian sleep has been implicated in maintaining a healthy extracellular environment in the brain. During wakefulness, neuronal activity leads to the accumulation of toxic proteins implicated in Alzheimer's disease. The glymphatic system is thought to clear these proteins by flushing cerebral spinal fluid (CSF) through the brain. In mice, this process occurs during non-rapid eye movement (NREM) sleep. And, in humans, increased ventricular CSF flow during NREM sleep, visualized using functional magnetic resonance imaging (fMRI), is also thought to be coupled to flow through the glymphatic system. But does waste clearance occur throughout sleep or is it specific to NREM sleep? Using fMRI of naturally sleeping pigeons, we show that REM sleep, a paradoxical state with wake-like brain activity, during which we experience our most vivid dreams, is accompanied in birds with the activation of brain regions involved in processing visual information, including optic flow during flight. We further demonstrate that, compared to NREM sleep, REM sleep is associated with a sharp drop in ventricular CSF flow. Consequently, functions linked to brain activation during REM sleep might come at the expense of waste clearance during NREM sleep.

Introduction

Sleep is a dangerous state of reduced environmental awareness thought to perform important functions for the brain. Recently, mammalian sleep has been implicated in maintaining a healthy extracellular environment in the brain[1]. During wakefulness, neuronal activity leads to the accumulation of toxic proteins, such as amyloid-β and tau, implicated in Alzheimer's disease[2–4]. The recently described glymphatic system[5] is thought to rectify this problem[1,6]. Specifically, cerebrospinal fluid (CSF) flows into the perivascular space along arteries penetrating the brain and enters the extracellular space, facilitated by the water channel aquaporin 4 (AQP4) on astrocytic endfeet[9], where it mixes with the interstitial fluid, and then drains via venous perivascular spaces, removing waste in the process[1]. Interestingly, as shown in mice, this process occurs during non-rapid eye movement (NREM) sleep[1]. In addition, although CSF flow into the brain has not been measured directly in sleeping humans, increased ventricular CSF flow, visualized using functional magnetic resonance imaging (fMRI), during NREM sleep is thought to be coupled to flow through the glymphatic system[7].

Several aspects of sleep's proposed role in clearing waste from the brain remain unresolved. Notably, it is unclear how CSF flow changes throughout the ventricular system and brain during REM sleep[6, 10–12], a paradoxical state with wake-like brain activity, during which we experience our most vivid, bizarre, story-like, and emotional dreams[8]. It is also unknown whether waste removal mediated by CSF flow through the brain is a general function of sleep shared by mammalian and non-mammalian species. Birds are well suited to address these questions. Despite last sharing a common ancestor with mammals over 300 million years ago, birds exhibit sleep states remarkably similar to mammalian NREM and REM sleep[13,14]. Although episodes of avian REM sleep are short (typically < 10 s) when compared to mammals, birds, such as pigeons, engage in hundreds of episodes per night. Importantly, birds are also

the only non-mammalian group to express AQP4 on astrocytic endfeet facing the blood vessels, a necessary cellular component of the glymphatic system[6,15]. Finally, as birds are homeotherms with high metabolic rates and large brains more densely packed with neurons than in mammals[16,17], they might have a greater need to clear metabolic waste from the brain.

Here we combined fMRI, EEG, and pupillometry in awake and naturally sleeped pigeons to probe brain mechanisms underlying REM and NREM sleeps. We show that brain regions involved in processing the visual world during wakefulness are activated during avian REM sleep. We further demonstrate that, as in mammals, ventricular CSF flow is greater during NREM sleep when compared to wakefulness. And, importantly, we show that REM sleep is coupled to a sharp drop in CSF flow throughout the ventricular system. Consequently, our findings suggest that a trade-off exists between functions performed by wide-spread brain activation during REM sleep and waste clearance during NREM sleep. Alternatively, we propose that despite impeding the flow of CSF into the ventricular system, the influx of blood into the brain during REM sleep might play an unexpected, complimentary role in moving fluids through the brain.

Results

Pigeons rapidly fall asleep inside the fMRI scanner after head fixation and cycle frequently between NREM and REM sleep

Before examining sleep state-dependent changes in CSF flow, we first established that avian REM sleep is associated with wide-spread brain activation. We measured whole brain BOLD from naturally sleeping pigeons (n = 15) in a 7T fMRI scanner and simultaneously acquired video recordings through an MR-compatible infra-red video camera (Fig. 1A). The birds were head-fixed using a chronically implanted plastic pedestal (Fig. 1A) to ensure a low level of head movements throughout the entire recording period. Only 0.2% of the volumes had frame-wise displacement higher than 0.09 mm (~ 20% of voxels size, fig. S1 and S2). Prior to the fMRI recording sessions, the birds underwent an extensive training procedure for progressive amounts of time (Fig. 1B) to reduce the stress associated with head fixation and scanner acoustic noise[18]. After completing the habituation, two of the recorded fMRI sleep sessions were analyzed. Using well-established behavioral correlates of EEG-defined NREM and REM sleep[14,19], we then identified all unambiguous bouts of NREM and REM sleep from the video recordings while blind to the corresponding fMRI signals. NREM was scored when both eyelids were closed and the eyes, pupils, and bill were still, whereas REM sleep was scored when both eyelids were closed, but the eyes, pupils, and/or bill were moving rapidly (see Materials and Methods, Movie S1). The birds had on average 85 bouts of NREM sleep (range 23–143) and 72 bouts of REM sleep (range 33–140; Fig. 1C). The number of NREM and REM sleep bouts was statistically similar for both recording sessions ($p_{NREM\ S1/S2}$ = 0.17, $p_{REM\ S1/S2}$ = 0.65; Fig. 1C).

BOLD fMRI responses during REM sleep reveal activity in most of the sensory and multi-sensory networks of the pigeon brain

We investigated the whole-brain activity patterns during REM sleep by analyzing REM > NREM sleep contrasts. As illustrated in Fig. 2, robust BOLD activation patterns within the telencephalon were found in most primary and all secondary sensory processing areas, as well as in multimodal integration regions. Within the hyperpallium, we found prominent activation clusters both in thalamopallial input areas (IHA, HI) as well as in associative structures (HD, HA) of the visual and the somatosensory hyperpallium. Within the dorsal ventricular ridge, primary visual (entopallium) and auditory areas (field L2) were active. In addition, associative areas of the trigeminal (NFT), the tectofugal visual (NIMl, NMm, NIL), and the auditory systems (fields L1, L3, NCM) demonstrated significant BOLD signal increases. We also observed significant activity in the convergence zones of both thalamo- and tectofugal visual pathways (NFL, TPO). In the higher-order mesopallial associative areas, the trigeminal (MFV), visual tectofugal (MIVl, MVL), auditory (MC), multimodal (MIVm), and limbic components (MFD) evinced significant activity patterns[20]. In addition, limbic areas like the nucleus accumbens (AC), parts of the septum laterale (SL), the bed nucleus of the stria terminalis (NSTL), and several subnuclei of the amygdala showed significant BOLD increases. Similarly, most of the anterior part of the prefrontal-like nidopallium caudolaterale (NCL)[21] the limbic-associative nidopallium caudocentrale (NCC) and the (pre)motor arcopallium (AI, AD) were active. While both hippocampal and parahippocampal areas did not evince significant BOLD signals, the area dorsolateralis cortcoidea (CDL) that closely interacts with the hippocampal formation was active[22]. At the subpallial level we found significant BOLD signals in lateral and medial striatum (StM, StL), globus pallidus (GP), and ventral pallidum (VP).

Within the diencephalon, the thalamic relay nuclei of the visual tectofugal (n. rotundus, Rt) and auditory pathways (n. ovoidalis, Ov) were activated along with the lateral hypothalamus and the n. dorsomedialis anterior (DMA) that corresponds to the intralaminar nuclei[25] and participates in the regulation of attention and arousal[26]. The brainstem pontomesencephalic reticular structures evinced significant BOLD responses that partly reached the deep layers of the tectum. Within the cerebellar cortex, we observed significant activity patterns in folia II to VI. All of the results were highly repeatable (fig. S4) and very similar to the REM vs baseline results (fig. S5, see Supplementary Material for ‘baseline’ definition), except that for this contrast, we could not detect significant BOLD signals in the hyperpallium.

Ventricular system of the pigeon shows increased fMRI signal during NREM sleep

In contrast to REM sleep, most of the significant fMRI signal associated with NREM sleep was located in the ventricular system or in the adjoining margins of the brain (Fig. 3). In the ventricles, it extended along the lateral ventricles englobing the caudal nidopallium, regionally in the third ventricle, and in the fourth ventricle, including its extension into the cerebellum, the cerebellar recess (CR)[27]. In addition, the interhemispheric fissure showed significant fMRI signal (Fig. 3). All results were repeatable across the two sessions (fig. S6) and similar to NREM vs baseline results (fig. S7). As in previous studies[7,11,28], we interpret these fMRI signals to reflect the inflow of CSF (see Supplementary Material). Finally, a bilateral cluster near the base of the telencephalon extended into the striatum in an area with large penetrating

arteries (Fig. 3, A 7.6), reflecting either activation of the neighboring striatum or CSF flow along these arteries.

Avian REM sleep is associated with BOLD activity surges in the telencephalon (gray matter) and sharp decreases in CSF inflow signal

To further understand the CSF dynamics, we focused on the BOLD-CSF relationship between NREM and REM sleep. The CSF and BOLD time-series were, respectively, extracted from the 4th ventricle (excluding the CR) located at the bottom slices (Fig. 4A, green mask), to maximize the sensitivity to the CSF inflow (as in [7] and [28])), and the telencephalon (Fig. 4A, red mask). As shown in a representative time series, the increases in the BOLD signal are linked to changes in the CSF signal, suggesting a strong coupling between the two (Fig. 4B). The cross-correlation results indicated a negative peak with a lag of + 4 s (Fig. 4C, -0.13, $p < 0.0001$ permutation test) which resembles a similar shape to that reported in humans[28]. This result confirmed the existence of significant temporal coupling between CSF and BOLD signals. We further calculated the average time course of the CSF and BOLD signals locked to the onset of bouts of NREM and REM sleep, and found that while the CSF flow signal during NREM sleep increased, the gray matter BOLD signal decreased (Fig. 4D). Interestingly, the opposite occurred in REM sleep; as the CSF flow signal decreased, the gray matter BOLD signal increased (Fig. 4E). In addition, the parameter estimates of the 4th ventricle and telencephalon were significantly different during NREM and REM sleep (Fig. 4F and 4G, NREM: $t(14) = -5.3$, $p < 0.0001$, paired-sample t-test; REM: $t(14) = -5.3$, $p < 0.0001$, paired-sample t-test). Finally, we examined how CSF flow changes between wakefulness and NREM sleep. As pigeons can engage in NREM sleep with open eyes[29], to ensure that they were awake, we presented sound stimuli shown to evoke typical waking EEG activity (fig. S8). As in mammals, birds showed reduced CSF flow during wakefulness compared to NREM sleep (fig. S9, $t(3) = 4.02$, $p < 0.01$, paired sample t-test). In addition, we analyzed the CSF signal from the cerebellar recess of the fourth ventricle (CR). The results confirmed the reproducibility of the BOLD-CSF coupling during sleep (fig. S10).

Discussion

The BOLD activity pattern during REM-sleep in pigeons shows remarkable similarities to results obtained in humans[30]. We observed significant activations in the mesopontine tegmentum, cerebellum, visual and intralaminar thalamus, amygdalar nuclei, further limbic and paralimbic structures, striatum, parts of the avian “prefrontal” structure, and most sensory and associative sensory areas of the pallium with the majority of these sensory areas being visual. This overlaps with findings in mammals[31–34]. Thus, the bilateral activation of primary and higher order visual regions in pigeons might support visual imagery during REM sleep[34], while activation of the amygdala suggests that such experiences involve emotions[30].

It is obviously unclear if pigeons experience dreams similar to humans[35]. With respect to the content of potential dreams, however, a very preliminary hypothesis could be formulated. When organisms move forward, they experience optic flow as a visual expansion in the direction of self-motion[36], while local

motion signals code for obstacles that should be avoided[37]. Such optic flow and local motion signals are integrated in the oculomotor cerebellum of which folia VI is a part[38]. Folia II-VI were also activated during REM sleep and further integrate tactile input from the whole-body surface of the bird, including the wings[39]. REM associated BOLD signals also covered those parts of the thalamic n. rotundus that are activated by optic flow and small moving objects[40]. These rotundal signals are then processed in the pallial visual tectofugal system and its associative visual areas[41], which were also active during REM sleep. Thus, it is tempting to speculate that our pigeons might have dreamed about scenes of flying while avoiding collisions with other objects.

Despite the similarity of the neural activation patterns of birds and mammals during REM sleep, two differences deserve attention. First, we did not observe an activation of the thalamic lateral geniculate nucleus that in mammals is part of the ponto-geniculo-occipital wave which constitutes a prominent phasic event during REM sleep[34]. Instead, the n. rotundus was activated in pigeons - a structure that constitutes the thalamic relay of the tectofugal visual pathway. Regarding memory processing, the absence of a mammal-like activation of the hippocampus and the parahippocampal region during REM sleep suggests that birds might process hippocampal information differently from mammals[42].

Although our findings indicate that functions linked to brain activation during REM sleep occur at the expense of ventricular CSF flow, REM sleep might still play an integral role in waste clearance. During the transition between NREM and REM sleep in rodents, the influx of blood into the brain[43] increases vascular diameter[44] and compresses the perivascular space through which CSF normally enters the brain[12]. This might restrict the entry of new CSF into the brain, and thereby account for the reduction in CSF flow outside the brain tissue in pigeons. However, at the same time, the increase in brain blood volume might squeeze the perivascular and extracellular spaces, thereby increasing flow through the brain tissue. Interestingly, as most of this flow should accompany the surge of blood at the onset of REM sleep, by engaging in hundreds of short episodes of REM sleep, rather than fewer and longer episodes, as in mammals, birds might maximize waste removal. Indeed, this partitioning of REM sleep into shorter episodes could be an evolutionary strategy to enhance waste clearance in avian brains with high neuronal density.

References

1. Xie, L. *et al.* Sleep drives metabolite clearance from the adult brain. *Science (80-.).* **342**, 373–377 (2013).

2. Kang, J. E. *et al.* Amyloid-β dynamics are regulated by orexin and the sleep-wake cycle. *Science (80-.).* **326**, 1005–1007 (2009).

3. Shokri-Kojori, E. *et al.* β-Amyloid accumulation in the human brain after one night of sleep deprivation. *Proc. Natl. Acad. Sci. U. S. A.* **115**, 4483–4488 (2018).

4. Winer, J. R. *et al.* Sleep Disturbance Forecasts β-Amyloid Accumulation across Subsequent Years. *Curr. Biol.* **30**, 4291-4298.e3 (2020).

5. Iliff, J. J. *et al.* A paravascular pathway facilitates CSF flow through the brain parenchyma and the clearance of interstitial solutes, including amyloid β. *Sci. Transl. Med.* **4**, (2012).

6. Rasmussen, M. K., Mestre, H. & Nedergaard, M. Fluid transport in the brain. *Physiological reviews* vol. 102 1025–1151 (2022).

7. Fultz, N. E. *et al.* Coupled electrophysiological, hemodynamic, and cerebrospinal fluid oscillations in human sleep. *Science (80-.).* **366**, 628–631 (2019).

8. Hobson, J. A., Pace-Schott, E. F. & Stickgold, R. Dreaming and the brain: Toward a cognitive neuroscience of conscious states. *Behav. Brain Sci.* **23**, 793–842 (2000).

9. Mestre, H. *et al.* Aquaporin-4-dependent glymphatic solute transport in the rodent brain. *Elife* **7**, (2018).

10. Tuura, R. O. G., Volk, C., Callaghan, F., Jaramillo, V. & Huber, R. Sleep-related and diurnal effects on brain diffusivity and cerebrospinal fluid flow. *Neuroimage* **241**, (2021).

11. Picchioni, D. *et al.* Autonomic arousals contribute to brain fluid pulsations during sleep. *Neuroimage* **249**, 118888 (2022).

12. Bojarskaite, L. *et al.* Sleep cycle-dependent vascular dynamics enhance perivascular cerebrospinal fluid flow and solute transport. *bioRxiv* 2022.07.14.500017 (2022) doi:10.1101/2022.07.14.500017.

13. Ungurean, G., van der Meij, J., Rattenborg, N. C. & Lesku, J. A. Evolution and plasticity of sleep. *Current Opinion in Physiology* vol. 15 111–119 (2020).

14. Rattenborg, N. C., Lesku, J. A. & Libourel, P. A. Sleep in Nonmammalian Vertebrates. in *Principles and practice of sleep medicine* (eds. Kryger, M. H., Roth, T., Goldstein, C. A. & Dement, W. C.) vol. 1 106–120 (Elsevier, 2022).

15. Yoshimura, K., Sugiura, K., Ohmori, Y., Aste, N. & Saito, N. Immunolocalization of aquaporin-4 in the brain, kidney, skeletal muscle, and gastro-intestinal tract of chicken. *Cell Tissue Res.* **344**, 51–61 (2011).

16. Olkowicz, S. *et al.* Birds have primate-like numbers of neurons in the forebrain. *Proc. Natl. Acad. Sci. U. S. A.* **113**, 7255–7260 (2016).

17. Kverková, K. *et al.* The evolution of brain neuron numbers in amniotes. *Proc. Natl. Acad. Sci. U. S. A.* **119**, e2121624119 (2022).

18. Behroozi, M. *et al.* Event-related functional MRI of awake behaving pigeons at 7T. *Nat. Commun.* **11**, 1–12 (2020).

19. Ungurean, G., Lesku, J. A. & Rattenborg, N. C. Sleep in birds. in *Reference Module in Neuroscience and Biobehavioral Psychology* (Elsevier, 2021). doi:10.1016/b978-0-12-822963-7.00081-5.

20. Atoji, Y. & Wild, J. M. Afferent and efferent projections of the mesopallium in the pigeon (Columba livia). *J. Comp. Neurol.* **520**, 717–741 (2012).

21. Güntürkün, O., von Eugen, K., Packheiser, J. & Pusch, R. Avian pallial circuits and cognition: A comparison to mammals. *Current Opinion in Neurobiology* vol. 71 29–36 (2021).

22. Atoji, Y. & Wild, J. M. Afferent and efferent connections of the dorsolateral corticoid area and a comparison with connections of the temporo-parieto-occipital area in the pigeon (Columba livia). *J. Comp. Neurol.* **485**, 165–182 (2005).

23. Karten, H. J. & Hodos, W. *Stereotaxic atlas of the brain of the pigeon (Columba livia)*. (The Johns Hophins Press, Baltimor, 1967).

24. Shanahan, M., Bingman, V. P., Shimizu, T., Wild, M. & Güntürkün, O. Large-scale network organisation in the avian forebrain: A connectivity matrix and theoretical analysis. *Front. Comput. Neurosci.* **7**, (2013).

25. Veenman, C. L., Medina, L. & Reiner, A. Avian Homologues of Mammalian Intralaminar, Mediodorsal and Midline Thalamic Nuclei: Immunohistochemical and Hodological Evidence. *Brain. Behav. Evol.* **49**, 78–98 (1997).

26. Montagnese, C. M., Mezey, S. E. & Csillag, A. Efferent connections of the dorsomedial thalamic nuclei of the domestic chick (Gallus domesticus). *J. Comp. Neurol.* **459**, 301–326 (2003).

27. Mestres, P. & Rascher, K. The ventricular system of the pigeon brain: a scanning electron microscope study. *J. Anat.* **184**, 35 (1994).

28. Han, F. *et al.* Reduced coupling between cerebrospinal fluid flow and global brain activity is linked to Alzheimer disease–related pathology. *PLoS Biol.* **19**, (2021).

29. Tobler, I. & Borbély, A. A. Sleep and EEG spectra in the pigeon (Columba livia) under baseline conditions and after sleep deprivation. *J. Comp. Physiol. A 1988 1636* **163**, 729–738 (1988).

30. Maquet. Functional neuroimaging of normal human sleep by positron emission tomography. *J. Sleep Res.* **9**, 207–231 (2000).

31. Maquet, P. *et al.* Functional neuroanatomy of human rapid-eye-movement sleep and dreaming. *Nature* **383**, 163–166 (1996).

32. Braun, A. R. *et al.* Regional cerebral blood flow throughout the sleep-wake cycle. An H215O PET study. *Brain* **120**, 1173–1197 (1997).

33. Nofzinger, E. A., Mintun, M. A., Wiseman, M., Kupfer, D. J. & Moore, R. Y. Forebrain activation in REM sleep: An FDG PET study. *Brain Res.* **770**, 192–201 (1997).

34. Miyauchi, S., Misaki, M., Kan, S., Fukunaga, T. & Koike, T. Human brain activity time-locked to rapid eye movements during REM sleep. *Exp. Brain Res.* **192**, 657–667 (2009).

35. Manger, P. R. & Siegel, J. M. Do all mammals dream? *Journal of Comparative Neurology* vol. 528 3198–3204 (2020).

36. Gibson, J. J. Visually controlled locomotion and visual orientation in animals. *Br. J. Psychol.* **49**, 182–194 (1958).

37. Wylie, D. R. Processing of visual signals related to self-motion in the Cerebellum of pigeons. *Front. Behav. Neurosci.* **0**, 4 (2013).

38. Gutiérrez-Ibáñez, C., Pilon, M. C. & Wylie, D. R. Pretecto- and ponto-cerebellar pathways to the pigeon oculomotor cerebellum follow a zonal organization. *J. Comp. Neurol.* **530**, 817–833 (2022).

39. Schulte, M. & Necker, R. Processing of spinal somatosensory information in anterior and posterior cerebellum of the pigeon. *J. Comp. Physiol. - A Sensory, Neural, Behav. Physiol.* **183**, 111–120 (1998).

40. Wang, Y. C., Jiang, S. & Frost, B. J. Visual processing in pigeon nucleus rotundus: Luminance, color, motion, and looming subdivisions. *Vis. Neurosci.* **10**, 21–30 (1993).

41. Stacho, M. *et al.* A cortex-like canonical circuit in the avian forebrain. *Science (80-.).* **369**, (2020).

42. Rattenborg, N. C., Martinez-Gonzalez, D., Roth, T. C. & Pravosudov, V. V. Hippocampal memory consolidation during sleep: A comparison of mammals and birds. *Biol. Rev.* **86**, 658–691 (2011).

43. Bergel, A., Deffieux, T., Demené, C., Tanter, M. & Cohen, I. Local hippocampal fast gamma rhythms precede brain-wide hyperemic patterns during spontaneous rodent REM sleep. *Nat. Commun.* **9**, 1–12 (2018).

44. Turner, K. L., Gheres, K. W., Proctor, E. A. & Drew, P. J. Neurovascular coupling and bilateral connectivity during nrem and rem sleep. *Elife* **9**, 1 (2020).

Methods

Animal Subjects. All experimental procedures were conducted under the National Institutes of Health Guidelines for the Care and Use of Laboratory Animals and were approved by the ethics committee of the State of North Rhine-Westphalia, Germany (Landesamt für Natur, Umwelt und Verbraucherschutz Nordrhein-Westfalen (LANUV), application number: Az.: 81-02.04.2021.A240). Fifteen adult domestic pigeons (*Columba livia*, Budapest highflyer variety; 7 females and 8 males, genetically sexed), obtained from a local breeder, were used in this study. Budapest pigeons were selected for this fMRI study

because their small body fits well in the small-bore of the preclinical scanner resonator. In addition, their large eyes and transparent eyelids allow pupil size and eye movements to be monitored even when the eyelids are closed[45]. Before the experiments, birds were reared and housed in enriched colony aviaries, under 12 h:12 h light:dark photoperiod, at 21 C. During the experiment, pigeons were individually housed in wire-mesh cages (45x45x45 cm^3) under the same photoperiod with *ad libitum* access to water and food.

Surgery and implantation. To prevent motion artifacts during the fMRI scans, all pigeons were implanted with an MR-compatible plastic pedestal. The protocol from our laboratory has already been published[18]. In summary, ketamine/xylazine (70% ketamine, 30% xylazine, 0.075 mL/100 g) was administrated intramuscularly in the breast muscle to anesthetize the birds before implantation. In addition, a supplement of gas anesthesia (Isoflurane; Forane 100% (V/V), Mark 5, Medical Developments International, Abbott GmbH and Co. KG, Wiesbaden, Germany) was administered. After fixing the pigeon's head in a stereotactic apparatus[23], the skin and soft tissues around the skull were removed and four polyether ether ketone (PEEK) micro pan head screws were screwed into the skulls to attach the custom-made plastic pedestal. In addition to the plastic pedestal, six birds were implanted epidurally over the hyperpallium with wire electrodes soldered to a connector. Two electrodes were placed over the visual hyperpallium of both hemispheres and the third one was placed above the cerebellum as a reference electrode. The electrodes and connector were embedded in biocompatible skin glue, covered by a thin layer of dental cement. Finally, custom-made plastic pedestals and screws were embedded with dental cement (OMNIDENT, Rodgau, Germany) to increase the adhesive strength between the skull and pedestal. Following each surgery, analgesic (carprofen (Rimadyl), Zoetis Deutschland GmbH, Berlin, Germany 10 mg/kg) and antibiotic (Baytril, Bayer Vital GmbH, Leverkusen, Germany, 2.5 mg/kg) treatments were given every 12 hours for at least 3 days. After a recovery period of 4–6 weeks with *ad libitum* access to water and food, the habituation training for head fixation started.

After recording the EEG signals, the electrodes were removed under isoflurane anesthesia (2-3% in one LPM oxygen) before running any fMRI scan to avoid interfering with fMRI signals.

Habituation procedure. To habituate the pigeons to the head fixation system (Fig. 1), they were gradually acclimated to the restrainer and acoustic noise of the magnet in a mock scanner using a well-established procedure in our laboratory[18,46,47]. This procedure helps to reduce the stress associated with head fixation and minimizes body motion artifacts. As a result of the procedure, the birds fell asleep after a few minutes inside the scanner. In brief, the habituation protocol consists of three main steps: (i) to habituate the animals to the experimental environment and the restrainer, pigeons were wrapped in a cloth jacket to prevent wing and leg movements and then placed in the restrainer inside the mock scanner in a dark room. (ii) to habituate the animals to the head fixation, animals were fixed to the holding device via the implanted MR-compatible plastic pedestal. The head fixation started with 10 min on the first day and was prolonged to 100 min in 12 days; (iii) to habituate pigeons to the scanner noise, a recorded single-shot Rapid Imaging with Refocused Echoes (RARE) sequence sound was replayed during head fixation with

gradually increasing sound pressure from 45 to 90 dB at one meter distance. After 18 days of habituation, the birds were ready to be restrained and scanned inside a real MRI machine.

EEG acquisition. Infrared (IR) illumination and IR-sensitive video cameras were used to monitor the sleep behavior. Video recordings were done at 30 fps. The EEG signal of the six birds implanted with electrophysiology electrodes was additionally recorded during the training phase at 256 Hz using the same recording system (Oneiros), as in our previous studies of Budapest pigeons[45,48,49].

fMRI acquisition. Prior to the main experiment, the EEG electrodes were removed from the 6 implanted birds, and the photoperiod was inverted to facilitate sleep recordings during the daytime. As pigeons, like diurnal mammals, engage more frequently in REM sleep later in the night[50], the fMRI recordings were performed in the second part of the birds' subjective night.

All MRI data collection was carried out in a Bruker BioSpec 7 Tesla scanner (horizontal bore, 70/30 USR, Avance III electronic, Germany) using Paravision 6.0 software. A quadrature birdcage resonator (82 mm ID) was used for RF transmission and a single-loop receiver surface coil (20 mm ID) was used for resting-state and anatomical data collection. By positioning the ring surface coil around the head, it was possible to reduce artifacts due to body movements. As changes in respiration may affect BOLD signals and brain connectivity maps, the respiration waveform was measured using a small pneumatic pillow placed under the pigeon's chest muscles (Small Animal Instruments, Inc. Model 1025T monitoring and gating system) during all resting-state measurements. The facial behavior of the animals was simultaneously recorded using an MRI-compatible video camera (12M-i, MRC Systems, Heidelberg, Germany; B/W) with an incorporated LED light (IR) (outside the pigeon's visible spectrum). To facilitate detection of changes in pupil size and eye position, a small mirror was placed next to each eye (Fig. 1A). The videos were acquired at 30 fps. All recordings including respiration signals, videos, and resting-state data were synchronized using a TTL signal.

To localize the correct position of the pigeon brain within the scanner bore, a series of scout images were measured at the beginning of each scanning session. Three runs (horizontal, coronal, and sagittal) were acquired using multi-slice rapid acquisition (RARE) with the following parameters: TR = 4 s, TEeff = 40.37 ms, RARE factor = 8, no average, acquisition matrix = 128 × 128, FOV = 32 × 32 mm, spatial resolution = 0.25 × 0.25 mm^2, slice thickness = 1 mm, number of slices = 20 horizontal, 17 sagittal, and 15 coronal. These images were used to orient 11 coronal slices to cover the entire telencephalon, optic lobes, midbrain, 4^{th} ventricle, and cerebellum.

Resting-State fMRI (rs-fMRI) data were acquired using a single-shot multi-slice RARE sequence adapted from Behroozi et al.[18,47], with the following parameters: TR = 4000 ms, TEeff = 41.58 ms, partial Fourier transform accelerator = 1.53, encoding matrix = 64 × 42, acquisition matrix = 64 × 64, FOV = 30 × 30 mm^2, in-plane spatial resolution = 0.47 × 0.47 mm^2, radio-frequency pulse flip angles for excitation and refocusing = 90°/180°, slice thickness = 1 mm, no slice distance, slice order = interleaved, excitation and refocusing pulse form = scanner vendor gauss512, receiver bandwidth = 50,000 Hz. To saturate the

signals from the eyes to avoid brain image corruption due to eye movements, two saturation slices were positioned manually over the eyes. Each run of the rsfMRI recordings included 1000 to 1450 volumes. To check the reproducibility and stability of the results, rsfMRI data of all animals were recorded twice on different days.

High-resolution T2-weighted anatomical images were acquired using a RARE sequence for better spatial normalization. Scan parameters were as follows: TR = 2000 ms, TEeff = 50.72 ms, RARE factor = 16, number of averages = 1, FOV = 25 × 25 × 15 mm^3, matrix size = 128 × 128 × 64, spatial resolution = 0.2 × 0.2 × 0.23 mm^3. The total scanning time was 17 min.

To represent the results in high-resolution anatomical images, following the final MRI data acquisition, one of the animals was deeply anesthetized with equithesin and transcranial perfused with a phosphate-buffered saline solution (PBS, 0.12M), followed by a mixture of paraformaldehyde (PFA 4%) and Dotarem® (1%). High-resolution 3D anatomical data was collected using a T2*-weighted sequence using a FLASH sequence with a flip angle of 15°, a spectral bandwidth of 50 kHz, 64 averages, a TR of 9.47 ms, a TE of 4.738 ms, and a scan repetition time of 5.000 ms. The images have a field of view of 25*25*20 mm^3 and an isotropic spatial resolution of 0.05 mm in all three directions. The recording time was ~ 20 h.

Awake condition. Since our birds closed their eyes and fell asleep almost immediately after head fixation, we had to wake them up. We, therefore, played loud auditory stimuli during the training EEG and fMRI acquisition. Auditory stimuli included a piece of classical music (first 8 s of Brandenburg Concerto No. 4 of Johann Sebastian Bach, compare supplementary sound S01) and two random chord stimuli centered at 1000 Hz (500–1500 Hz) and 3000 Hz (1500–4500 Hz). The auditory stimuli were presented using an MR-compatible speaker (SoundCraft) which was placed at a distance of 8 cm from the tip of the bill. In total, 45 trials were played during the EEG and fMRI recordings. Each trial consisted of 8 s auditory stimuli followed by 52 s of silence. We digitized all stimuli at 44.1 kHz. The maximum sound pressure level (SPL) was approximately 90 dB (measured at a 1 cm distance from the speaker).

Sleep state scoring. The sleep states were manually scored using the video recordings. To facillitate the scoring process, actimetry signals were calculated for the eyes, irises, and bill region and visualized together with the video recordings. NREM sleep was characterized by bilateral eye closure, stable breathing (as visible in the videos and bill actimetry signals), immobility of the eyes, and absence of bill movements other than those related to breathing. REM sleep was characterized by bilateral eye closure with movements of the eyes, bill, and/or the collapse of head feathers held erect during preceding NREM sleep. As described previously[45], rapid constrictions and dilations of the iris are closely associated with REM sleep. Thus, rapid iris movements were also used to identify bouts of REM sleep and their absence to confirm NREM sleep.

EEG data processing. The EEG data was analyzed using custom Matlab (v2020b) scripts. First, a time-frequency analysis using a multitaper method (*9*) was performed for the complete recordings session using the following parameters: F_{min} = 0, F_{max} = 40Hz, window size = 4s, step = 50ms, band

width = 1Hz, taper number = 3, pad = 1. A time window of 40s centered on the sound onset was exctracted for stimulation trial. The signals were averaged across trials to obtain an average time-frequency representation. To calculate the average power spectrum associated with the auditory stimulation, the signal was averaged across the 8 s of stimulation. A similar averaging was done for a 8-s time window prior to the stimulation.

BOLD fMRI data processing. All fMRI data processing was performed using tools from the FMRIB Software Library (https://fsl.fmrib.ox.ac.uk/fsl/fslwiki/FSL, version 5.0.9), the Analysis of Functional NeuroImages (AFNI, version 20.0.09 https://afni.nimh.nih.gov/), and Advanced Normalization Tools (ANTs, http://stnava.github.io/ANTs/) software. A standard pipeline was used to pre-process the rsfMRI data. Prior to any preprocessing steps, the DICOM images were converted to 4D NIFTI data (using the *dcm2nii* function), and the voxel size was upscaled by a factor of 10 (using the *3drefit* function of AFNI). The censoring of high motion frames was applied to estimate the amount of head movement within each resting-state time series[51]. The threshold for framewise displacement (i.e., volume to volume movement) was set as 0.9 mm (less than 20% of voxel size). The results indicated that only 25 volumes of all 29 rs-fMRI sessions had an FD-value higher than 0.9 mm (after upscaling voxel size by a factor of 10). Later, the following standard data preprocessing steps were applied: (i) motion correction using MCFLIRT[52] (FSL's intra-modal motion correction tool), (ii) slice time correction (interleaved acquisitions, using the *slicetimer* function), (iii) skull stripping of functional data (using a BET[53] and manual cleaning), (iv) spatial smoothing (using *3dBlurInMask* function with FWHM of 8 mm, after upscaling), (v) global intensity normalization by a single multiplicative factor for each scan run (for group analysis), (vi) high-pass temporal filtering (using the *3dTproject* function, with cutoff at 0.01Hz). The first 5 and last 5 volumes were discarded to ensure longitudinal magnetization reached a steady state and also to avoid the edge effect of temporal filtering. To consider the respiratory-related artifacts, voxel-wise regressors for physiological noise based on respiratory signals were generated using the PNM tool in FSL[54] by calculating the respiratory phases relative to each volume and slice in the rs-fMRI signals.

We then co-registered each rs-fMRI data to the corresponding T2-weighted anatomical images using affine linear registration (12 degrees of freedom). A population-based template was generated using *antsMultivariateTemplateConstruction.sh* script[55]. After analyzing individual subjects, the results were normalized to the population-based template using FMRIB's Nonlinear Image Registration Tool (FNIRT)[56] for group analysis. For visualizing the results, the group results were non-linearly warped to the high-resolution post-mortem anatomical image. 3D MRI images were visualized using the MANGO software (http://ric.uthscsa.edu/mango/, version 4.1).

ROI definition. The fourth ventricle (IV), its extension into the cerebellum, namely the cerebellar recess (CR), and the gray matter mask were defined anatomically in the high-resolution anatomical image (from the perfused animal). The brightest voxels in the anatomical image were selected to identify the position of IV and CR. The CSF masks were selected from the bottom slices of the rs-fMRI data to ensure high sensitivity of the 2D rs-RARE images to the CSF through-slice inflow effect as mentioned previously[7,28].

Since there is no blood in the CSF regions, the fMRI signal changes in these regions are mainly due to variations of the inflow of fresh spins into the imaging volume[7,57]. This inflow effect size is much stronger at the edge of the imaging volume because the fresh spins arriving have not yet experienced magnetization saturation due to the radiofrequency pulses[57]. We, thus, extracted the CSF signals from the voxels within lower slices[7,28] to estimate an index of the change in CSF flow over time.

ROIs for the BOLD signal in the gray matter were defined by two spheres with a diameter of 65 mm (after upscaling by a factor of 10) on both hemispheres (centered at the Entopalium) to include most of the telencephalon. We transformed the selected masks from the high-resolution anatomical space to the functional space of each pigeon using the reversed concatenated transformation matrix from the previous steps. However, the masks in the functional space were also visually inspected to ensure their correct position. All ROI analyses and value extraction were done within the fMRI acquisition space of each pigeon to avoid any spatial blurring of the original fMRI signal during transforming into the template space.

Statistics and reproducibility. All linear mixed model analyses were performed in R using the *lmer* package. The other statistical tests were performed in MATLAB (v2020b). The level of statistical significance was set to $p < 0.05$. The number of NREM and REM sleep bouts in the two analyzed sessions was tested using a paired Student's t-test. To assess whether the sound stimulation (to awaken the birds) influenced the EEG activity in the hyperpallium (the primary visual area), we calculated the average power in the delta band (0.5-4 Hz) 20 s before and during the stimulation (fig. S8). The effect of the stimulation was calculated using linear mixed effect models, with the average delta power before, or during the stimulation as the response variable, the condition (stimulation vs non-stimulation) as a predictor, and the bird identity as a random effect.

Whole-brain statistical analysis was carried out using FEAT (FMRI Expert Analysis Tool, a part of FSL) with high-pass temporal filtering (cut-off 100 s) and pre-whitening using FILM[54] on individual pigeons. The general linear model (GLM) included a regressor for each of the NREM and REM sleep bouts and their temporal derivatives. In addition to the two regressors of the NREM and REM sleep blocks and to the PNM regressors (to account for the effects of physiological noise in the BOLD signal), six scan-to-scan estimated motion parameters, and frames that exceeded a threshold of 0.9 mm FD (to account for any residual effects of animal movement) were added as confounds in the GLM model. The experimental regressors of interest were used to create the following brain activity contrasts for the different sleep stages: positive and negative main effects of REM versus NREM sleep phases, as well as REM versus baseline and NREM versus baseline; baseline includes the other scored sleep state, plus the unscored periods with open eyes that can include wakefulness and NREM sleep[29].

Out of the 15 pigeons, 14 had two recording sessions, and one had only one. The experiments were run on two independent days. Each session was analyzed independently. A two-sample paired t-test (implanted in FSL) was used to reveal potential changes in activity on the first and second days. Since there was no significant difference between the two sessions (fig. S4 and S6), within-subject effects

(across the two days) were then established in second-level analysis (fixed effects) to average the two sessions from each pigeon.

For the group analysis, contrasts of interest from second-level analyses were then taken into the higher-level analysis using the nonparametric FSL's *Randomise* function[58]. Statistical significance was assessed using permutation testing with 5,000 permutations, Threshold-Free Cluster Enhancement (TFCE), and a family-wise error (FWE) corrected cluster p-value of p = 0.05.

GM and CSF signal analysis. In addition to the mentioned preprocessing steps, the "*film_gls*" and "*fsl_regfilt*" functions were used to regress out the voxelwise explanatory variables of respiration signal and estimated motion parameters (3 translations and 3 rotations), respectively. To have equal fluctuation amplitudes, the fMRI signals were normalized to Z-score at each voxel. For each resting-state session, the mean fMRI signals from each mask were extracted. For the ROI signal analysis of GM and CSF as a function of time and sleep state, we selected NREM/REM bouts whose onset were a minimum of 12 s away from NREM/REM bout offsets to minimize any possible effect of the adjacent NREM and REM bouts on each other.

Data availability

Functional MRI and anatomical images of awake and sleep pigeons can be accessed via https://ruhr-uni-bochum.sciebo.de/s/Xi80mw1EB0qySAU.

Code availability

FSL (https://fsl.fmrib.ox.ac.uk/fsl/fslwiki/FSL, version 5.0.9), the Analysis of Functional NeuroImages (AFNI, version 20.0.09 https://afni.nimh.nih.gov/), and Advanced Normalization Tools (ANTs, http://stnava.github.io/ANTs/) software and MATLAB (v2020b, MathWorks, USA) were used to process fMRI and EEG data. Codes for fMRI data processing are available at https://github.com/mehdibehroozi/sleeping_pigeon_fMRI.

References

45. Ungurean, G., Martinez-Gonzalez, D., Massot, B., Libourel, P. A. & Rattenborg, N. C. Pupillary behavior during wakefulness, non-REM sleep, and REM sleep in birds is opposite that of mammals. *Curr. Biol.* **31**, 5370-5376.e4 (2021).

46. Behroozi, M. *et al.* In vivo measurement of T 1 and T 2 relaxation times in awake pigeon and rat brains at 7T. *Magn. Reson. Med.* **79**, 1090–1100 (2018).

47. Behroozi, M., Ströckens, F., Helluy, X., Stacho, M. & Güntürkün, O. Functional Connectivity Pattern of the Internal Hippocampal Network in Awake Pigeons: A Resting-State fMRI Study. *Brain. Behav. Evol.* **90**, 62–72 (2017).

48. Massot, B. *et al.* ONEIROS, a new miniature standalone device for recording sleep electrophysiology, physiology, temperatures and behavior in the lab and field. *J. Neurosci. Methods* **316**, 103–116 (2019).

49. Ungurean, G., Barrillot, B., Martinez-Gonzalez, D., Libourel, P. A. & Rattenborg, N. C. Comparative Perspectives that Challenge Brain Warming as the Primary Function of REM Sleep. *iScience* **23**, 101696 (2020).

50. Martinez-Gonzalez, D., Lesku, J. A. & Rattenborg, N. C. Increased EEG spectral power density during sleep following short-term sleep deprivation in pigeons (Columba livia): Evidence for avian sleep homeostasis. *J. Sleep Res.* **17**, 140–153 (2008).

51. Power, J. D. *et al.* Methods to detect, characterize, and remove motion artifact in resting state fMRI. *Neuroimage* **84**, 320–341 (2014).

52. Jenkinson, M., Bannister, P., Brady, M. & Smith, S. Improved optimization for the robust and accurate linear registration and motion correction of brain images. *Neuroimage* **17**, 825–841 (2002).

53. Smith, S. M. *et al.* Advances in functional and structural MR image analysis and implementation as FSL. in *NeuroImage* vol. 23 (Neuroimage, 2004).

54. Brooks, J. C. W. *et al.* Physiological noise modelling for spinal functional magnetic resonance imaging studies. *Neuroimage* **39**, 680–692 (2008).

55. Avants, B. B., Tustison, N. & Song, G. *Advanced Normalization Tools (ANTS)*. www.picsl.upenn.edu/ANTS. (2011).

56. Andersson, J. L. R., Jenkinson, M. & Smith, S. M. Non-linear optimisation. FMRIB technical report TR07JA1. *Pr.* 16 (2007).

57. Gao, J. H. & Liu, H. L. Inflow effects on functional MRI. *Neuroimage* **62**, 1035–1039 (2012).

58. Winkler, A. M., Ridgway, G. R., Webster, M. A., Smith, S. M. & Nichols, T. E. Permutation inference for the general linear model. *Neuroimage* **92**, 381–397 (2014).

Declarations

Acknowledgments

This work was supported by grants from Max Planck Society (GU, LB, NCR), Deutsche Forschungsgemeinschaft (DFG, German Research Foundation) – Projektnummer 316803389 – SFB 1280 (OG), and AVIAN MIND, ERC-2020-ADG, LS5, GA No. 101021354 (OG). The authors are grateful to the animal care staff at the Max Planck Institute for Biological Intelligence and Ruhr University Bochum for taking care of the birds.

Author contributions

The lead contributors are listed first, in alphabetical order, and marked with *. The other contributors are listed in alphabetical order. Conceptualization: NCR*, GU*. Methodology: MB*, GU*, P-AL, XH. Investigation: MB*, GU*, LB. Visualization: MB*, GU, LB. Funding acquisition: OG*, NCR*. Project administration: GU*, MB, OG, NCR. Supervision: OG*, NCR*. Writing – original draft: MB*, OG*, NCR*, GU*. Writing – review & editing: MB*, OG*, NCR*, GU*, LB, P-AL, XH.

Competing interests

Authors declare that they have no competing interests.

Figures

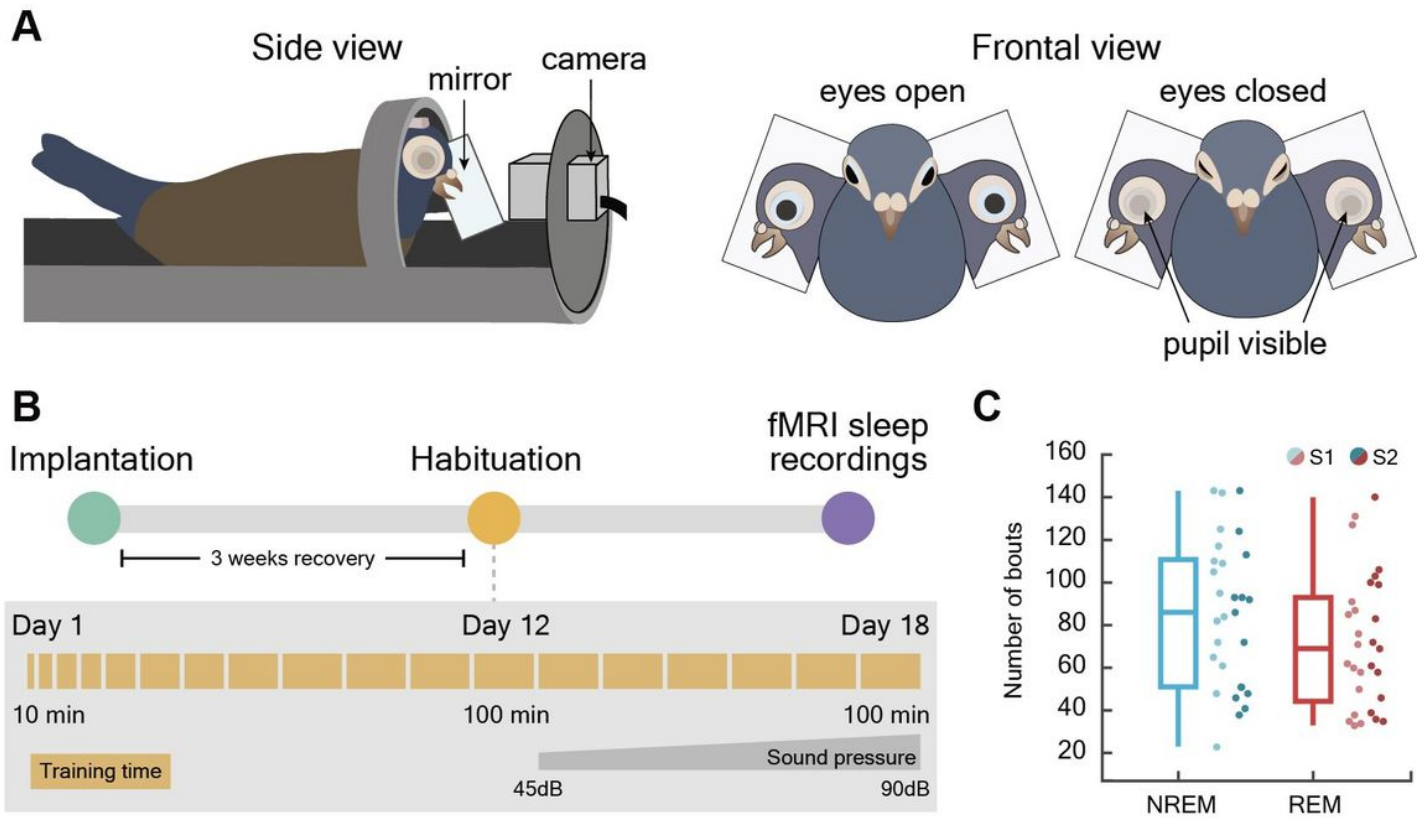

Figure 1

Measuring naturaly occurring NREM and REM sleep in pigeons inside a 7T scanner.(**A**) Experimental setup. Head-restrained pigeons (n=15) were positioned in the center of the scanner bore and their eyes, pupils, and bill were monitored using an MR-compatible camera. Two mirrors were placed bilaterally to cover both eyes using a single camera. (**B**) Before running the main experiment, pigeons underwent 18 days of habituation to the scanner setup. (**C**) To test the reproducibility of the results, each pigeon was scanned in two independent sessions. The number of NREM and REM sleep bouts was similar on both days. The sessions are coded with bright (session 1, S1) and dark (session 2, S2) colors. Each dot represents the number of NREM/REM bouts for a single bird.

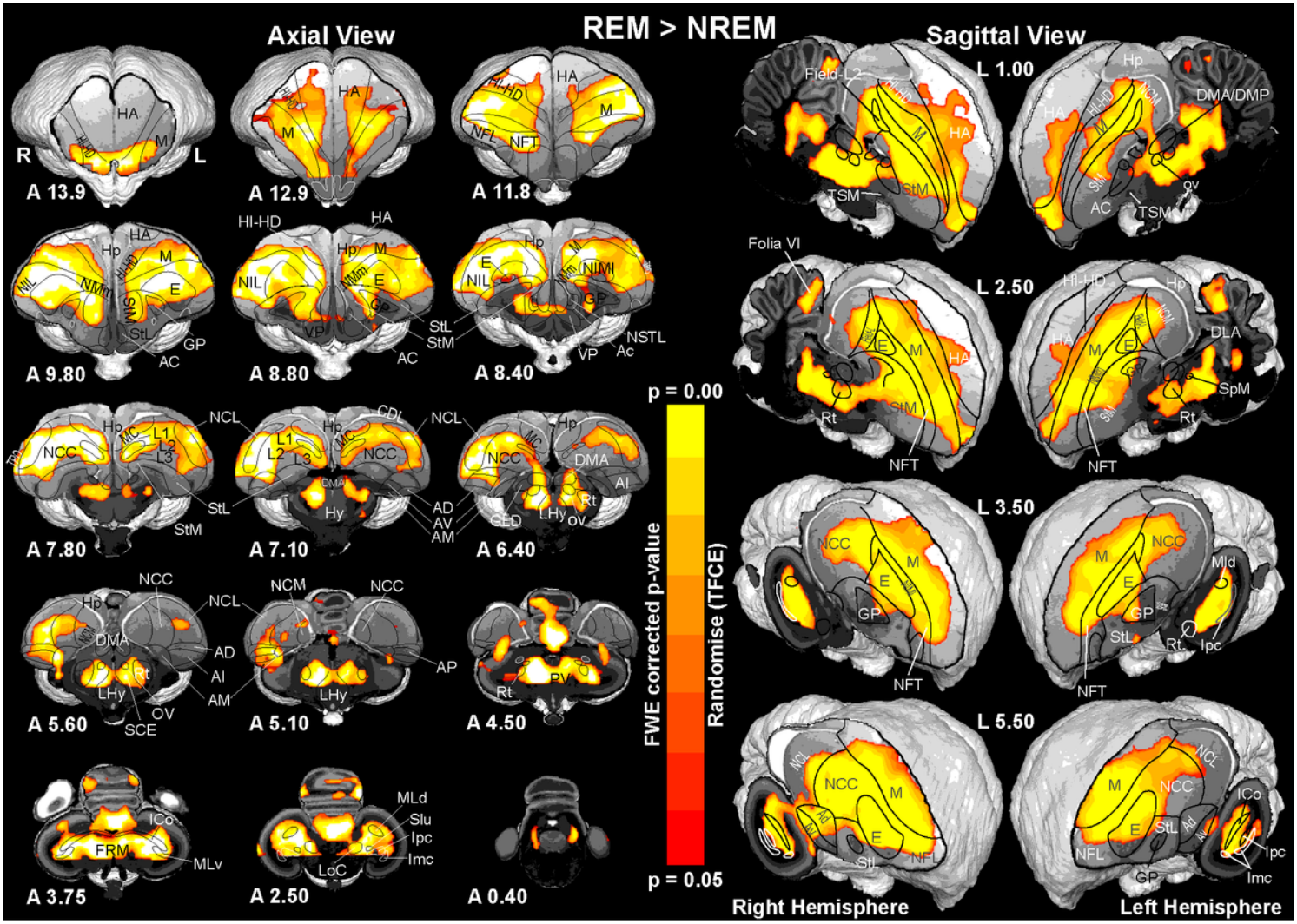

Figure 2

Brain activation patterns during REM sleep. A GLM analysis was used to demonstrate the activated networks during REM sleep phase by examining the REM > NREM contrast. The pigeon-specific hemodynamic response function[18] was used to optimize the modeled BOLD responses. The left panel shows the activation pattern of group-averaged data from 15 pigeons (29 sessions) in the axial view (group analysis using a nonparametric method, “randomise”, 5,000 permutations, Threshold-Free Cluster Enhancement, and a family-wise error corrected cluster p-value of p = 0.05). Functional maps were

overlaid on the high-resolution anatomical data at the different levels of an ex-vivo pigeon brain (in greyscale). The right panel represents the same activation pattern during REM sleep in the sagittal views. The activation significance is demonstrated by the color scale. Anatomical borders (black and white lines) are based on the contrast difference in the ex-vivo Budapest pigeon brain, the pigeon brain atlas [23], and the telencephalic connectome of the pigeon forebrain[24]. The corresponding abbreviations of delineated ROIs are listed in Table S1. Frontal and sagittal slice coordinates are defined based on the Budapest pigeon's brain anatomy (fig. S3).

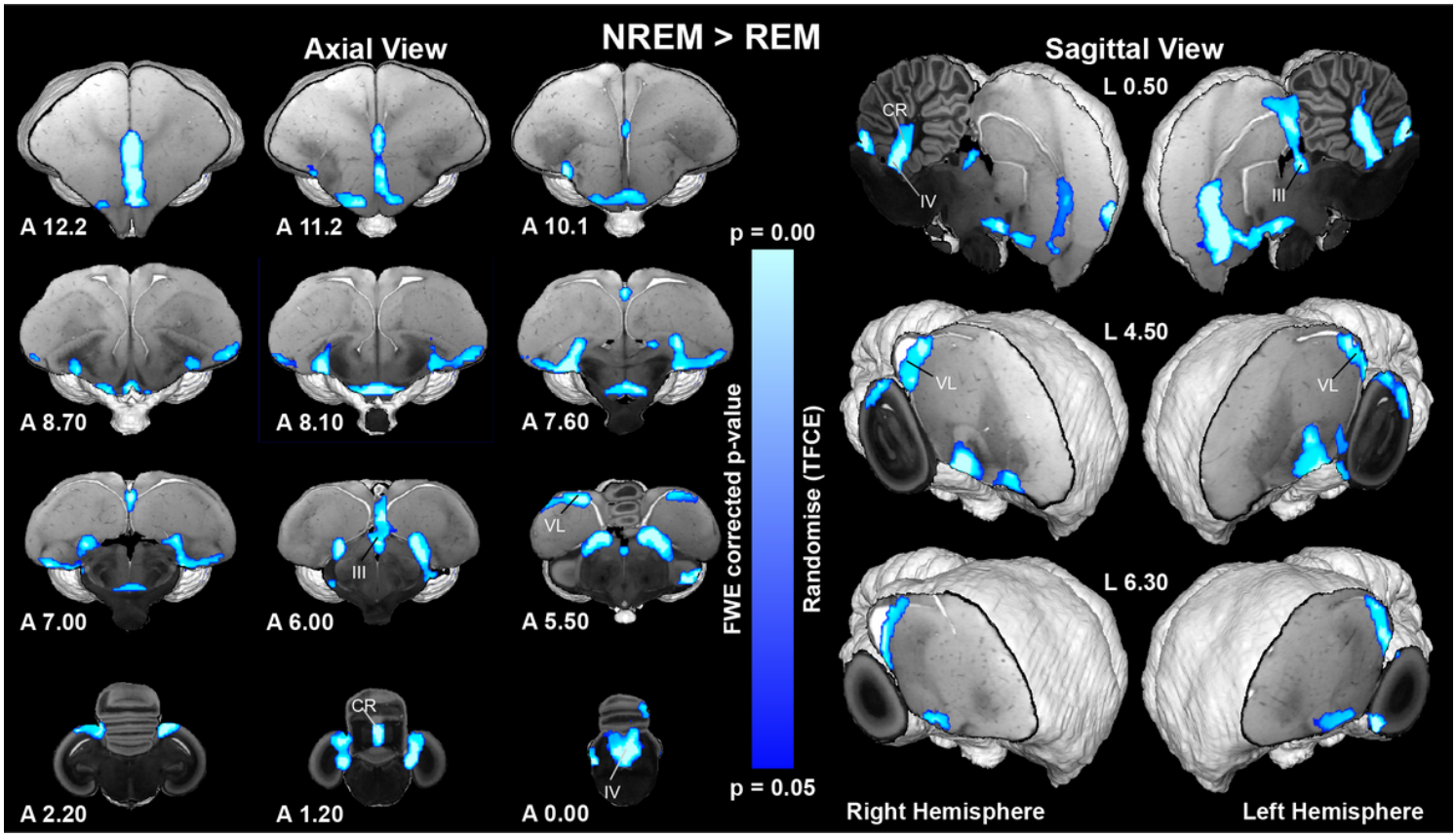

Figure 3

Increased fMRI signal associated with NREM sleep. The high-resolution axial and sagittal slices at the different levels of an ex-vivo pigeon brain are in greyscale, while the contrast map represents the significant increase of fMRI signal during the NREM sleep (NREM > REM contrast, n= 15 pigeons, 29 sessions). Group analysis was done using a nonparametric method, "randomise" with 5,000 permutations, Threshold-Free Cluster Enhancement, and a family-wise error corrected cluster p-value of p = 0.05. The significance of the fMRI signal increase is demonstrated by the color scale. The corresponding abbreviations of delineated ROIs are listed in Table S1. Frontal and sagittal slice coordinates are defined based on the Budapest pigeon's brain anatomy (fig. S3).

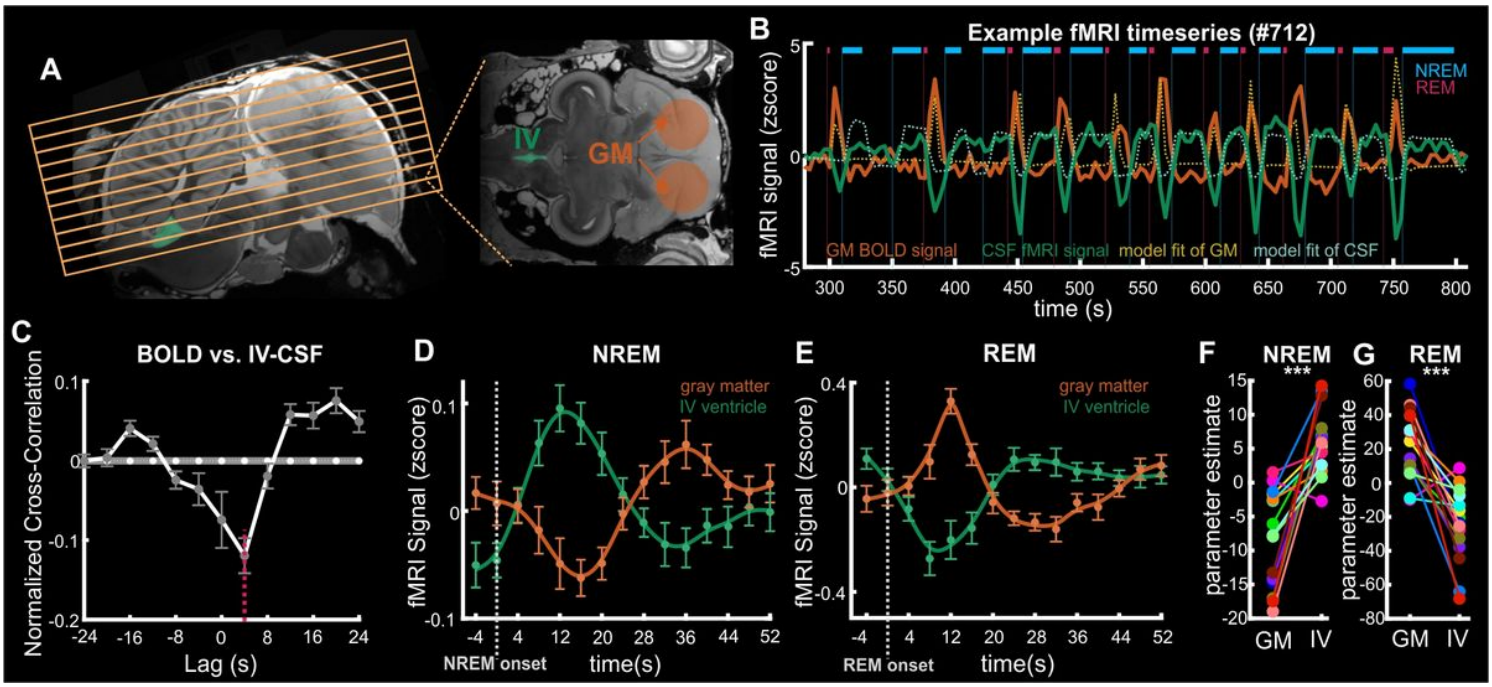

Figure 4

Association between BOLD signal in the telencephalon (gray matter) and CSF inflow signal. (**A**) Position of acquired functional slices (yellow grid) and selected ROIs (orange and green masks) relative to the high-resolution anatomical image. The BOLD signal was extracted from the voxels in the pigeon's telencephalon (orange mask, a sphere with a diameter of 6.5 mm centered at the entopallium to cover most of the telencephalon). The CSF signal was averaged from the IV ventricle (excluding the cerebellar recess), at the bottom slices of the fMRI acquisition (green mask). (**B**) Representative example time-series of the telencephalic BOLD and CSF signals depicting changes in both signals relative to bouts of NREM and REM sleep. During sleep, the BOLD signal dynamics are anticorrelated to the CSF signal. The BOLD signal increases during REM sleep when CSF flow decreases. The CSF flow increases during NREM sleep when the BOLD signal decreases. (**C**) Mean cross-correlation between BOLD and CSF signals (n=29, 15 pigeons). The negative cross-correlation at +4 s lag demonstrates the strongest coupling between BOLD and CSF signal (-0.13, $p<0.0001$ permutation test, red dashed line). The white dashed line and gray shaded region represent the mean correlation at each time lag and the 95% confidence interval of shuffled data. Error bars denote the standard error of the mean (SEM) across different lags. (**D, E**) Average time courses in BOLD and CSF signals locked on NREM and REM sleep onset, respectively. Error bars represent SEM. (**F, G**) Parameter estimates during the NREM and REM sleep (n=15). Colored circles show the average beta estimate over the GM mask and IV ventricle mask for each bird. CSF inflow increases compared to the BOLD signal during NREM sleep ($t(14)=5.4$, $p<0.00001$, paired-sample t-test), and the opposite occurs during REM sleep ($t(14)=-5.3$, $p<0.0001$, paired-sample t-test).

Supplementary Files

This is a list of supplementary files associated with this preprint. Click to download.

- SupplementaryInformationUngureanBehroozietal.pdf
- SupplementarMovie1.mp4